


Flexible capacitive pressure sensors with porous double microstructured layers

Jun Wang¹, Hanxuan Sun¹, Shenghua Chen¹, Ce Xu², Zhihua Wang³ 

¹Hebei University of Technology, The State Key Laboratory of Reliability and Intelligence of Electrical Equipment, Tianjin, China.

²The China Petroleum LIAOHE Equipment Company, Panjin City, China.

³Hebei University of Technology, Tianjin, China.

e-mail: 1312349729@qq.com, 15122695177@163.com, chenshenghua@hebut.edu.cn, xuce2001@163.com, wangzhihua@hebut.edu.cn

ABSTRACT

In this study, a flexible capacitive pressure sensor was developed, featuring a dielectric layer composed of a polydimethylsilane (PDMS)/BaTiO₃/SrTiO₃ composite material. The electrode and dielectric layers were structured with a dual microstructure, combining diagonal and sandpaper-porous elements. Additionally, nano-barium titanate (BT) powder, known for its relatively high dielectric constant, was incorporated into PDMS, along with an appropriate amount of strontium titanate (STO), to enhance the sensor's sensitivity. The developed sensor exhibited a remarkable sensitivity of 2.681 kPa⁻¹, with response and release times of approximately 39 ms and 61 ms, respectively. It demonstrated a low detection threshold and withstood over 5000 compression cycles, showcasing excellent repeatability. The results underscored the sensor's robust pressure-sensing performance, making it suitable for diverse applications, including human pulse monitoring, heartbeat tracking, robot arm sensing, object weight detection, and real-time healthcare monitoring.

Keywords: Flexible Capacitive Sensor; Double Microstructure Layer; Nano-Barium Titanate; Multi-Walled Carbon Nanotubes; Pressure Sensor.

1. INTRODUCTION

The rapid advancement of electronic skin, intelligent manipulators, human-computer interaction, and wearable devices has fueled a substantial demand for flexible sensors that exhibit remarkable ductility and adaptability [1–4]. Consequently, the need for acquiring essential data has gained significant attention, resulting in diverse requirements for flexible pressure sensors. Several types of flexible pressure sensors have emerged, each based on distinct signal conversion mechanisms, including resistive [5, 6], capacitive [7, 8], piezoelectric [9–12], triboelectric [13, 14], and fiber-optic [15, 16]. Among these, capacitive pressure sensors have attracted substantial interest owing to their noteworthy advantages, including high sensitivity, rapid response, and low power consumption, prompting extensive research in this domain [17–20].

Historically, research endeavors have primarily concentrated on enhancing critical parameters such as sensor sensitivity and flexibility. Some researchers have expanded the contact area between the electrode and the dielectric layers while increasing the variation in plate distance to augment the sensor's measurement range and sensitivity within specific pressure ranges. However, it is important to note that larger sensors are less practical for real-world applications [21]. Presently, two widely adopted strategies exist for enhancing sensor performance. One strategy revolves around the utilization of surface microstructures or porous structures to reduce the material's modulus, thus enhancing the overall deformability of the sensor. For this purpose, various methods have been devised, including bionic microstructures, 3D printing, and electrospinning [17, 22–26]. Additionally, researchers have implemented folded electrode structures, which have demonstrated commendable sensitivity, stable performance, and outstanding ductility. Notably, a study introduced a high-tensile electrode composed of copper nanowires and polydimethylsiloxane (PDMS) elastic films, enabling the sensor to maintain optimal performance even under stretching conditions [27].

Furthermore, the incorporation of materials possessing higher dielectric constants has the potential to elevate the overall performance of capacitive pressure sensors. The introduction of high-performance ceramic materials such as calcium copper titanate (CCTO) and barium strontium titanate [(Ba, Sr)TiO₃] in polymer

functional composites has yielded positive results [28–30]. Composite films with porous structures, fabricated using flexible materials like polydimethylsiloxane (PDMS), polyurethane (PU), and vulcanized silicone rubber, have showcased exceptional sensing properties. These advancements in composite materials have opened new avenues for selecting dielectric layer materials. Furthermore, the integration of array structures and the diversification of sensor applications in research have broadened the prospects for sensor utilization.

In this study, we developed a pressure sensor with a “sandwich” structure, incorporating multi-walled carbon nanotubes (CNTs) [31, 32] as the electrode material. This development aimed to enhance the detection limit, reduce costs, and improve the ductility of flexible pressure sensors (FCPS). The dielectric layer is composed of polydimethylsiloxane (PDMS) composites doped with nano-barium titanate (BT) and strontium titanate (STO). To ensure the sensor’s adaptability, we have introduced a double microstructure combination, consisting of the diagonal microstructure in the electrode layer and the porous sandpaper microstructure in the dielectric layer. Subsequently, we have conducted a theoretical analysis and testing of the sensor’s response to pressure. Finally, the sensor has been applied to the skin to evaluate its performance in detecting various signals, including gesture changes and pulse patterns.

2. SENSOR PREPARATION

2.1. Electrode preparation

Ecoflex silicone rubber, renowned for its insulating properties and flexibility, serves as an ideal material for crafting flexible sensor substrates. The electrode layer of the sensor was created by coating the Ecoflex layer’s surface with multi-walled carbon nanotubes (CNTs). Figure 1(a) illustrates the preparation process.

Initially, the dispersion solution was dissolved in deionized water, placed in a warm water bath. Subsequently, 3wt.% of multi-walled CNTs were added and thoroughly stirred to ensure complete infiltration of the CNTs by the aqueous dispersant solution. After undergoing 30 min of ultrasonic dispersion treatment, we obtained the multi-wall CNTs solution. Meanwhile, the A/B components of the Ecoflex silicone rubber, mixed in a 1:1 mass ratio, were placed in a container to eliminate bubbles over approximately 20 min. The silicone rubber was then spun onto a glass substrate, shaping the slanted structure by employing the reverse mold of the slanted substrate created through 3D printing. Following this, the multi-wall CNTs solution was applied to the structure and subsequently cured at 70°C for 3 h, resulting in the preparation of the sensor electrode.

The conductive film of the capacitive pressure sensor exhibited adequate flexibility and conductivity, serving as both upper and lower electrode substrates. Notably, when the carbon nanotube concentration was low, the electrode demonstrated superior tensile properties. However, as the concentration of CNTs increased, the tensile properties of the electrode decreased, accompanied by an increase in fracture load. Furthermore, higher CNT concentration led to greater CNT reunion on the silicone rubber substrate, causing uneven distribution and elevated tensile strength of the electrode, thereby diminishing its elasticity. The conductive stability was influenced by the variable thickness of the conductive network. At lower carbon nanotube concentrations, the distribution of CNTs on the flexible electrode’s surface was sparse, resulting in fewer interconnected nodes in the conductive network. Conversely, with an increase in CNT concentration, a sufficiently thick conductive network formed on the surface, causing minimal disruption to the conductive path during the tensile process and maintaining relatively stable conductive performance. As depicted in Table 1, when comparing the performance of different carbon nanotube concentrations, the overall performance of the electrode was optimal at a carbon nanotube concentration of 2wt.%.

2.2. Preparation of dielectric layer

The addition of strontium titanate and barium titanate increases Young’s modulus of PDMS. Because the amount of curing agent can affect the softness of PDMS after curing, a 10:1 PDMS ratio is unsuitable for the dielectric

Table 1: Tensile properties and electrical conductivity of carbon nanotubes with different concentrations.

CONCENTRATION	1WT%CNTS	2 WT%CNTS	3 WT%CNTS
PROPERTY			
Tensile property	1.7MPA	1.8MPA	1.85MPA
Fracture load	1000%	920%	860%
Electrical conductivity	0.13S/CM	0.42S/CM	0.62S/CM

layer. Therefore, different ratio schemes were compared and analyzed in this study to ensure both flexibility and desirable dielectric properties of the dielectric layer.

PDMS materials were prepared at ratios of 12:1, 13:1, and 14:1, and 25wt% of barium titanate and strontium titanate were added to PDMS. The resulting mixtures were uniformly coated on a clean glass plate and cured at 70°C for 4 h. A ratio of 13:1 was deemed more suitable because it resulted in satisfactory flexibility with high ceramic material content without excessive viscosity, resulting in hindered release while exhibiting excellent recovery performance.

The PDMS and curing agent were divided into five parts at a ratio of 13:1. Different mixtures containing 5%, 10%, 15%, 20%, and 25% of strontium titanate and barium titanate were added, along with an appropriate amount of pure sodium chloride. The mixtures were thoroughly blended for 30 min and then placed in a vacuum environment for 20 min to remove bubbles. Subsequently, these samples were spun onto a sandpaper (500-mesh) template and left at 70°C for 2 h to solidify the dielectric layer. Thereafter, the prepared dielectric layer was soaked in pure water for 2 h, resulting in the precipitation of sodium chloride, followed by drying. The resulting dielectric layer exhibited a sandpaper microstructure. The preparation process is depicted in Figure 1(b).

2.3. Characterization and measurement

2.3.1. Surface morphology of sensor electrode layer and dielectric layer

The surface morphology of the sensor's dielectric layer was analyzed through optical microscopy and SEM to examine the specific states of the electrode layer and node layer of the prepared sensor, as depicted in Figure 2. The dielectric layer exhibited a porous structure, and the surface exhibited sandpaper microstructure, consistent with the experiment's expected requirements. Additionally, a re-examination of the electrode surface revealed a distinct diagonal surface structure with attached CNTs.

2.3.2. Data collection

The surface morphology of the porous dielectric layer was analyzed through field emission scanning electron microscopy (SEM) [Zeiss-SIGMA HD] and optical microscopy [Ningbo Shunyu-ICX41 series]. Figure 3(a) provides a schematic diagram of the sensor structure. As illustrated in Figure 3(b), the sensor data acquisition system was operated as follows: First, the signal generator was used to generate the corresponding sinusoidal signal, which was then amplified by the power amplifier to drive the exciter. The force sensor at the end of the exciter transmitted a signal to the pressure acquisition system through the acquisition card. The force sensor relayed a signal to the tactile sensor, changing its capacitance. The change in capacitance was detected using an impedance analyzer [KEYSIGHT E4990A, China], which was operated within a frequency range of 20 Hz to 10 MHz.

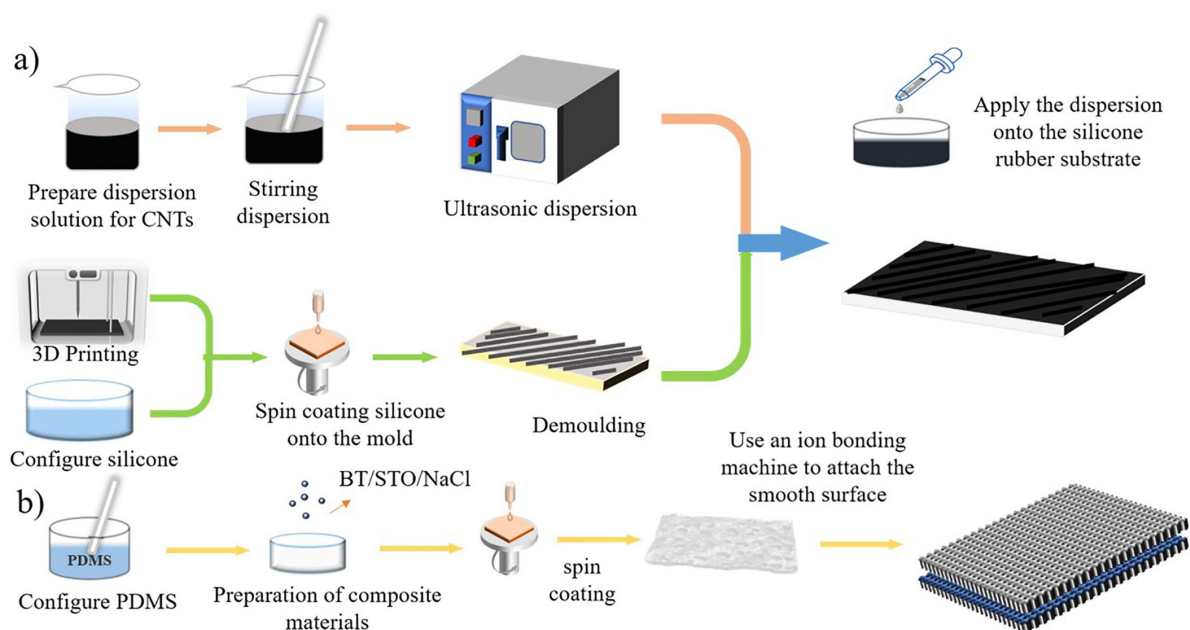


Figure 1: (a) Sensor electrode preparation process. (b) Sensor dielectric layer preparation process.

2.4. Sensor assembly

As illustrated in Figure 3(a), the sandwich-structured flexible pressure sensor consisted of an Ecoflex silicone rubber substrate, a multi-walled CNT electrode, and a PDMS/BaTiO₃/SrTiO₃ dielectric layer. The smooth surfaces of the dielectric layer were bonded together using an ion bonding machine to form a complete two-sided dielectric layer. Copper strips were also bonded to the contact electrodes, facilitating the evaluation of sensor performance using connecting wires.

In this study, the diagonal microstructured electrode layer was combined with the sandpaper microstructured porous dielectric layer. To confirm that the performance of the designed structure was superior, planar dielectric layers, porous dielectric layers, and sandpaper microstructure dielectric layers were prepared simultaneously to evaluate the sensitivity of the sensors with different structures.

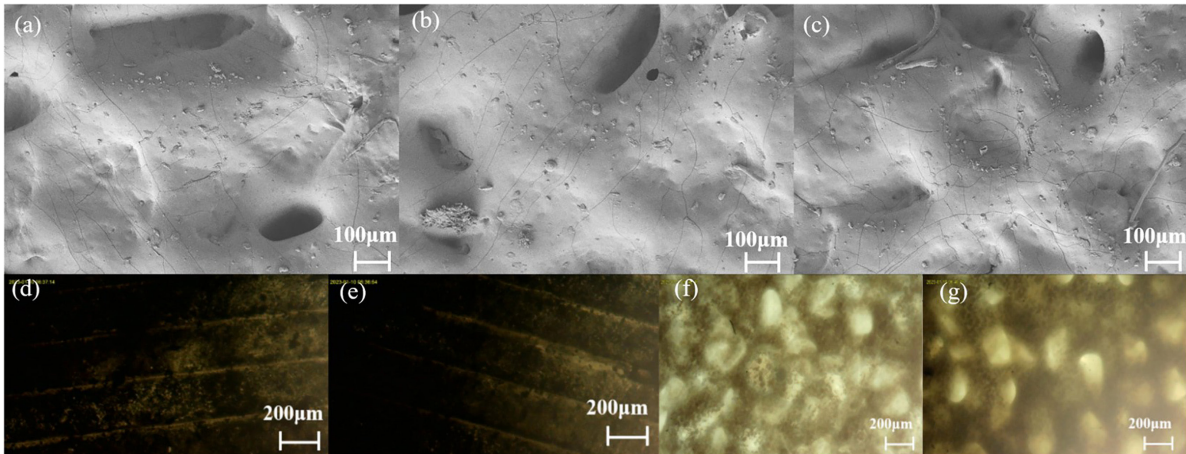


Figure 2: (a–c) Dielectric layer field emission scanning electron microscope. (d–e) Dielectric layer optical microscope. (f–g) Electrode layer optical microscope photograph.

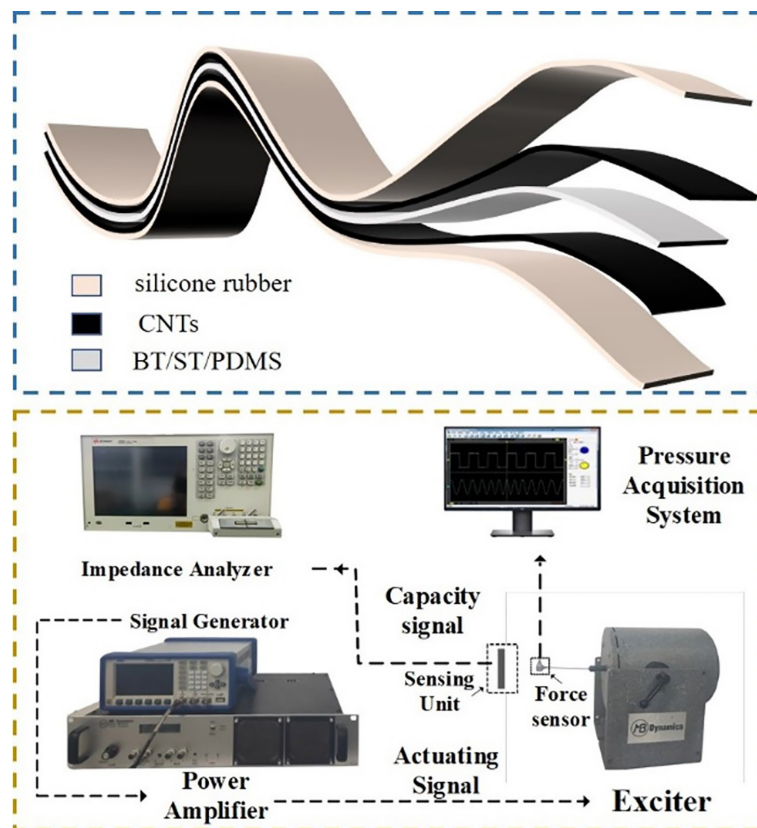


Figure 3: (a) Schematic diagram of sensor structure hierarchy. (b) Data acquisition system.

3. RESULTS AND DISCUSSION

3.1. Analysis of the working principle of pressure sensor

The capacitive sensor developed in this study adheres to a conventional “sandwich” structure, comprising a flexible dielectric layer sandwiched between two layers of flexible parallel plate electrodes. Figure 4(a) provides a schematic depiction of the sensor’s response to stress changes, and the sensor’s capacitance value is calculated using equation (1):

$$C = \frac{\epsilon A}{4\pi kd} \quad (1)$$

where k is the electrostatic constant, which has a value of approximately 8.988×10^9 . The capacitance value C is inversely proportional to the electrode distance d and directly proportional to the dielectric constant ϵ and the area A of the two plates. When external pressure is applied, compressing the dielectric layer and reducing the distance between the two electrodes, the capacitance value increases. The sensitivity S of the capacitive pressure sensor is calculated using equation (2):

$$S = \frac{\Delta C / C_0}{P} \quad (2)$$

where ΔC represents the capacitance change ($C - C_0$), C_0 denotes the initial capacitance, and P denotes the applied pressure.

The sensor employs a dielectric layer with surface microstructure and a porous structure. In the initial state, an air gap exists between the electrode and the dielectric layers, as shown in Figure 4(b), facilitating the sensor’s deformation under pressure and increasing the effective electrode area. The dielectric constant ϵ is related to the volume components of air and the dielectric layer as per equation (3):

$$\epsilon = \epsilon_{air} \cdot V_{air}\% + \epsilon_d \cdot V_d\% \quad (3)$$

where ϵ_{air} and $\epsilon_{dielectric}$ denote the initial relative permittivity of air and the dielectric layer, and V_{air} and $V_{dielectric}$ denote the volume percentages of air and the dielectric layer, respectively. When pressure is applied to the sensor, the volume proportion of air decreases while the volume proportion of the dielectric layer increases. As represented by Equations (1), (2), and (3), when the pressure applied to the sensor surface reaches a certain threshold, the electrode layer and the dielectric layer tightly bond and approach a size of zero. As the dielectric constant of air is significantly lower than that of the PDMS composite dielectric layer, even slight pressure changes can result in substantial alterations in the capacitance value.

The microstructure of the electrode makes there is an air gap between the two poles of the capacitor sensor, which affects the capacitance value in the process of deformation caused by pressure. Because the electrode surface structure is regular linear, the positive opposite area of the upper and lower plates gradually increases during the pressing process. When the pressure reaches the critical value and the microstructure of the electrode layer and dielectric layer is compressed to the limit, the positive opposite area of the plate reaches the maximum value. The relative change of capacitance is shown in equation (4):

$$\frac{\Delta C}{C_0} = \frac{C_1 - C_0}{C_0} = \frac{\epsilon \frac{A + \Delta A}{d - \Delta d}}{\epsilon \frac{A}{d}} = \frac{d(A + \Delta A)}{A(d - \Delta d)} \quad (4)$$

Where Δd is the change in plate spacing and ΔA is the change in contact area.

3.2. Performance test of the pressure sensor

The sensor’s sensing performance was assessed by applying vertical external pressure. As illustrated in Figure 2(b), the sensor was firmly affixed to the test platform using insulation tape to prevent slippage. An impedance analyzer measured the sensor’s capacitance in real time, with a measurement frequency of 1 MHz, ensuring a relatively stable range of measured capacitance values. The sensing performance of dielectric layers with different surface structures was measured, as shown in Figure 5(a). The capacitance change rates of sensors with planar, sandpaper microstructured, and porous structures were recorded under various pressures.

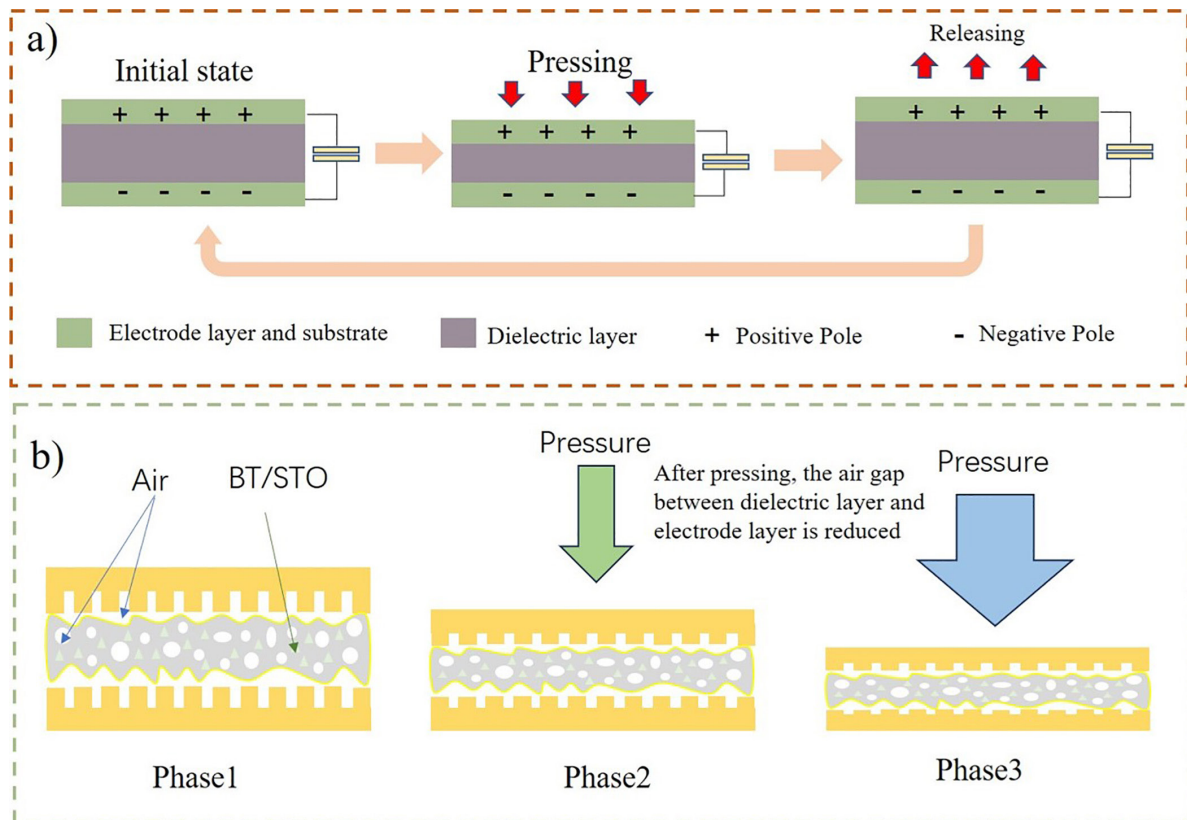


Figure 4: (a) Schematic diagram of sensor stress deformation. (b) Surface topography change.

As illustrated in Figure 5(a), within the range of 0–3 kPa, the sensor sensitivity of the porous structure reached 0.351 kPa^{-1} , while the sandpaper microstructure sensor exhibited a sensitivity of 0.303 kPa^{-1} . The composite structure sensor achieved a remarkable sensitivity of 0.713 kPa^{-1} , substantially higher than that of the planar structure (0.021 kPa^{-1}). In the 3–7 kPa range, sensors with surface microstructures continued to perform well, while the capacitance of planar structure sensors remained relatively stable. Consequently, the sensor with the porous sandpaper composite microstructure as the dielectric layer demonstrated optimal performance.

This study fabricated sensors with varying BT/STO contents (5%, 10%, 15%, 20%, 25%) in the dielectric layers, labeled FCPS-5, FCPS-10, FCPS-15, FCPS-20, and FCPS-25. The corresponding initial capacitance values of these sensors were 8.45 pF, 10.35 pF, 11.74 pF, 14.03 pF, and 15.17 pF, respectively, as depicted in Figure 5(b).

Prior research and preliminary studies have suggested that doping ceramic materials into the dielectric layer to enhance the sensor's dielectric constant can improve its sensitivity. The exceptional flexibility and low Young's modulus of PDMS make it an ideal material for flexible sensor fabrication. The dielectric properties of PDMS can be significantly improved by incorporating materials like BT/STO. Furthermore, by adjusting the mass ratio, a dielectric layer with desirable dielectric properties and flexibility can be achieved. As illustrated in Figure 5(c), doping with BT/STO substantially enhances the sensor's performance. The sensor performance of FCPS-10 surpassed that of ordinary microstructured sensors. However, FCPS-15 achieved a sensitivity of 0.832 kPa^{-1} within the pressure range of 0–3 kPa, surpassing FCPS-10. With a 20% BT/STO content, FCPS-20's performance substantially improved, resulting in a sensor sensitivity of up to 2.681 kPa^{-1} . Furthermore, it retained a sensitivity of 0.412 kPa^{-1} even when the pressure increased to 3–5 kPa. Comparing a series of 10% to 20% energy curves, it is evident that increasing the dielectric constant leads to increased sensitivity. However, beyond a 25% content, the performance improvement is not significant, and sensitivity slightly decreases, possibly due to the high ceramic material content, which affects the sensor's compression performance. Due to the excessive addition of ceramic materials, the Young's modulus of the composite material is too high. Under the same pressure, the dielectric layer shape variable is smaller, resulting in a larger polar distance D . Because the capacitance value is affected by the dielectric constant and polar distance, the sensor performance deteriorates when the ceramic material content is 25wt% or above. FCPS-5 was excluded from further investigation because its capacitor size and dielectric properties could not be compared with the other sensors. Considering both

sensitivity and flexibility, the dielectric layer with 20% BT/STO content was selected for sensor fabrication. The sensor accurately detected different pressures when subjected to successive normal forces of 0.3 kPa, 1.2 kPa, 2.6 kPa, and 5.0 kPa, as shown in Figure 5(d). Figure 5(e) illustrates the results of small force tests when 1, 2, and 3 lightweight coins were repeatedly placed on the sensor, producing minor capacitance changes, effectively detecting slight pressure signals. Furthermore, as depicted in FIG. 5(f), after exposing the sensor to low-temperature, room-temperature, and high-temperature environments, the sensing signal remained relatively stable, affirming the sensor's stability.

Table 2 is the important performance comparison of various flexible capacitive pressure sensors. The sensor prepared in this paper has a relatively large range, high sensitivity and short response time, and has excellent performance in all aspects.

Performance indicators such as response time, release time, durability, and other factors hold significance in sensor assessment. In Figure 6(a), we observe the sensor's response to a 1 kPa force applied under the influence of an exciter, involving 6000 cycles of detection experiments. The two magnified insets in

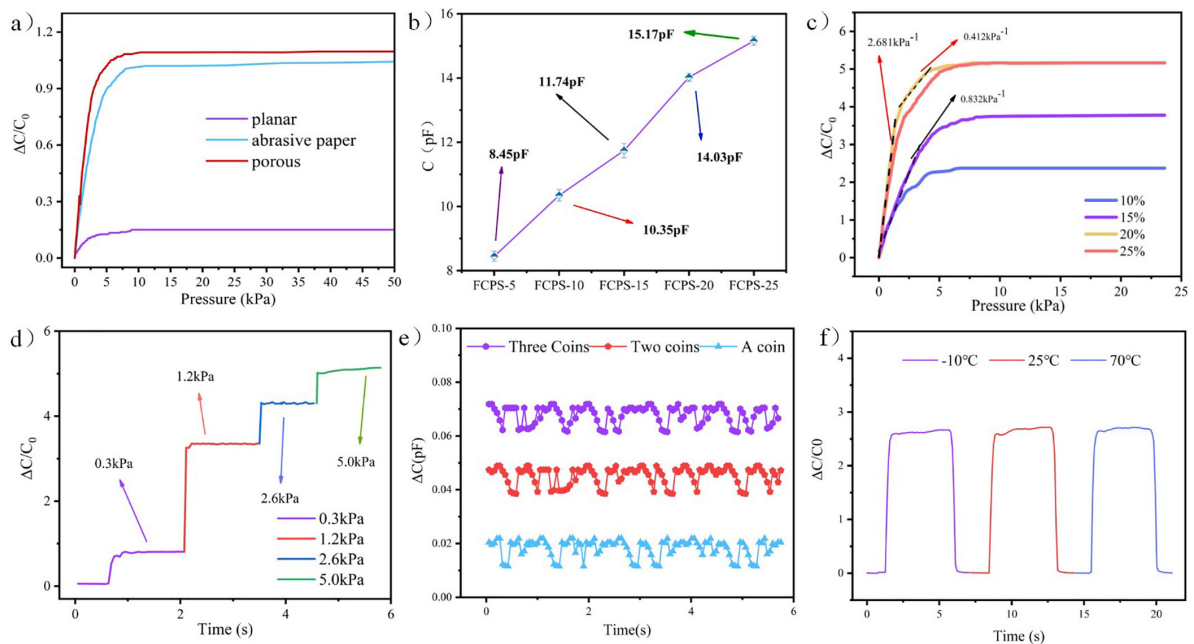


Figure 5: (a) Sensitivity comparison of planar structure, porous structure, sandpaper microstructure and composite structure sensors. (b) Comparison of the initial capacitance of sensors with different dielectric material contents. (c) Comparison of the sensitivity of sensors with different dielectric material contents. (d) Comparative analysis of different pressure conditions of FCPS-20. (e) Place light coins. (f) Capacitance changes at different temperatures.

Table 2: Performances comparison of different tactile sensors.

ELECTRODE	DIELECTRIC LAYER	MEASURING RANGE (KPA)	MAXIMUM SENSITIVITY (KPA ⁻¹)	RESPONSE TIME (MS)	REFERENCE
CNTs	CNTs	0–3.5	2.13	<100	[33]
activated carbon non-woven fabrics	graphene/PS microsphere/PDMS	0–150	0.209	<25	[34]
CuNWs/PDMS	porous PDMS	0–6	0.162	<240	[27]
Al fabric	porous PDMS composites	0–400	0.18	<100	[35]
copper tape	CNT/BT@DCPU	0–100	2.51	<100	[36]
CNTs/silicon rubber	PDMS/BT/STO	0–50	2.681	35	本文

Figure 6(a) depict the relative capacitance change curves at the experiment's commencement and conclusion. Despite numerous loading and releasing cycles over an extended period, the sensor's compression and release times exhibited slight changes. The relative capacitance consistently and stably changed, with no notable performance degradation. Even after 6000 detection cycles, the sensor maintained its excellent sensing performance. The sensor's performance was affected by the viscosity of PDMS and elastic fatigue due to multiple loading and releasing cycles.

To evaluate the sensor's response and release times, we recorded the capacitance changes under applied pressure using an impedance analyzer, as shown in Figure 6(b). The experimental sensor FCPS-20 displayed a small response time of approximately 39 ms and a release time of approximately 61 ms. These results indicate that the developed sensor possesses rapid response, good durability, high stability, and reliable recovery performance.

In Figure 6(c), we subjected the sensor to forces of the same magnitude but at different frequencies to assess its response. A force of 1 kPa was applied at frequencies of 1 Hz, 2 Hz, 3 Hz, and 5 Hz, respectively. Even when the force frequency increased to 5 Hz, the capacitance response curve remained stable. These test outcomes confirm that the prepared sensor can consistently generate stable signals when subjected to pressures below 5 Hz.

Additionally, an important parameter of the sensor is the hysteresis characteristic, as displayed in Figures 6(d) and (e) concerning load and unload cycles in terms of capacitance changes. The relative capacitance curves under loading pressure and unloading pressure almost entirely overlapped. Figure 6(d) presents the capacitance change curve at the start of the cyclic loading and unloading experiment. Under applied pressure, the relative capacitance change exhibited minimal variation, rendering hysteresis effects negligible in these sensors. As shown in Figure 6(e), the relative capacitance displayed minimal changes for applied pressures within the 2–6 kPa range, with significant overlap in other pressure ranges. These experimental results underscore that the as-prepared pressure sensor possesses robust durability and desirable repeatability, making it suitable for various complex working environments.

3.3. Applicability of the pressure sensor

The prepared sensor can be applied in scenarios involving significant strains. When attached to a computer mouse button, as depicted in Figure 7(a), the sensor detects continuous or intermittent capacitance changes

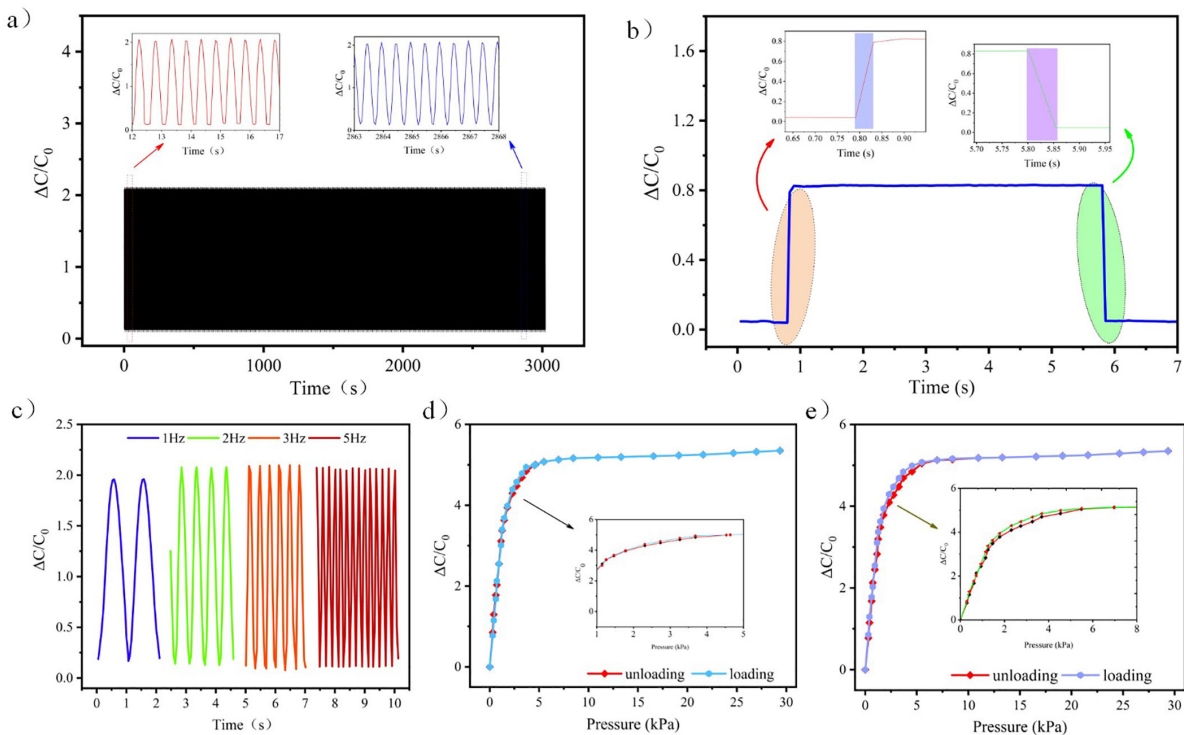


Figure 6: (a) Reliability test of cyclic detection. (b) Response release time. (c) Response of sensor to forces of different frequencies. (d) Hysteresis characteristic curve of cyclic detection before the experiment. (e) Hysteresis characteristic curve of cyclic detection after the experiment.

when the button is clicked or pressed. Thus, placing the sensor on both mouse keys enables real-time monitoring of mouse clicks. Figure 7(b) illustrates the sensor affixed to the fingertip of a glove's index finger and thumb. Robust relative capacitance signals are detected when gripping a water cup. Moreover, stable signals are generated when picking up and putting down the cup. As the cup's water level increases, a stronger force is required to stabilize it when it's half-full or full (empty cup mass: 3.94 g, half-full cup mass: 82.57 g, full cup mass: 176.66 g). The relative change rates of capacitance change were 0.2, 0.4, and 0.6, respectively, indicating the sensor's stable response to varying forces. When the sensor was initially mounted on the hand's knuckle, gradually increasing the finger's bending angle resulted in signal increases, indicating different signal responses to various angles (30°, 60°, and 90°), as shown in Figure 7(c).

The high sensitivity of FCPS-20 under low-pressure conditions enables effective detection of small pressures. Figure 7(e) demonstrates that when the sensor is attached to the throat, distinct relative signal changes occur during swallowing actions such as drinking and eating. Figure 7(d) presents five prominent peaks and several small pulses within 5 s. Furthermore, throat movement causing pressure on the sensor results in a capacitance change rate of approximately 18%, leading to significant signal alterations. In Figure 7(f), the FCPS-20 sensor is placed on the carotid artery to measure pulse parameters, with the results shown in Figure 7(g). The sensor generates regular signal fluctuations under pulse stimulation, exhibiting good stability and consistent measurement capabilities. The pulse rate is approximately 73 pulses/min, within the normal range of a human heartbeat. Figure 7(h) displays three distinct peak parameters, P1, P2, and P3, in the pulse waveform, suitable for medical analysis to calculate clinical parameters and serve as indicators for human health monitoring and early warning. Additionally, during intense physical exercise, the pulse rate significantly increases to approximately 110 pulses/min, accompanied by a large fluctuation in signal magnitude and a

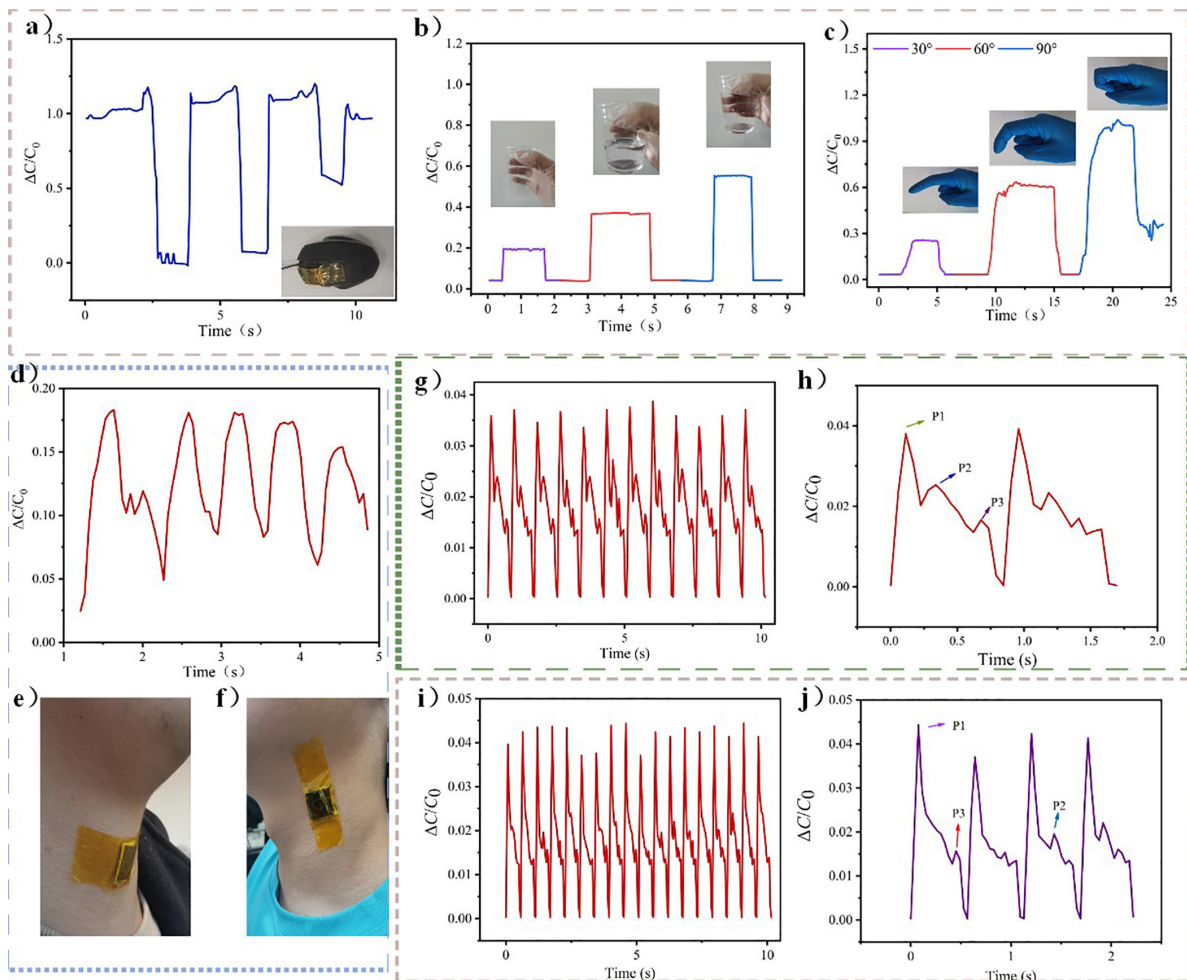


Figure 7: (a) Mouse button click. (b) Glass pinch. (c) Finger bending. (d) Swallowing signal. (e) Sensor attached to the throat. (f) Sensor attached to the artery. (g) Normal pulse conditions. (h) Normal pulse conditions. (i) Pulse after physical activity. (j) Pulse after physical activity.

maximum change rate of approximately 17%, as illustrated in Figures 7(i) and (j). Thus, the sensor's ability to detect low-amplitude pressure changes is evident when measuring pulse parameters. Therefore, the FCPS-20 sensor, as prepared, possesses a low detection limit and can measure certain small parameters.

4. CONCLUSIONS

In this study, a porous capacitive sensor was developed using PDMS with double microstructures, featuring a dielectric layer with a porous sandpaper microstructure and a sensor electrode with diagonal CNTs microstructures. This sensor demonstrated significant performance improvements in comparison to conventional planar sensors. To enhance the dielectric properties and flexibility of the dielectric layer, barium titanate (BT) and strontium titanate (STO) were introduced to create a BT/STO/PDMS composite material. Consequently, the dielectric layer exhibited an exceptionally high relative dielectric constant while maintaining high elasticity, leading to enhanced sensor performance. When the doping material content was increased to around 20%, the resulting sensor displayed a remarkable sensitivity of 2.681 kPa^{-1} , with minimal response and release times of approximately 39 ms and 61 ms, respectively. Furthermore, the sensor exhibited a low detection limit and demonstrated resilience, enduring more than 6000 compression cycles with only minimal signal attenuation. These findings underscore the sensor's high durability and reliability. Through testing, the developed sensor showcased its versatility by accurately estimating the weight of objects, detecting physiological signals such as human swallowing and pulse, and effectively capturing various gesture signals. These attributes position the sensor as a suitable choice for a wide array of applications in healthcare and wearable devices.

5. BIBLIOGRAPHY

- [1] GE, D., BABANGIDA, A.A., HU, Z., *et al.*, "Flexible pressure sensor based on a thermally induced wrinkled graphene sandwich structure", *IEEE Sensors Journal*, v. 22, n. 4, pp. 3040–3051, 2022. doi: <http://doi.org/10.1109/JSEN.2021.3130445>.
- [2] MIN, S., KIM, D.H., JOE, D.J., *et al.*, "Clinical validation of wearable piezoelectric blood pressure sensor for continuous health monitoring", *Advanced Materials*, v. 35, n. 26, pp. e2301627, Mar. 2023. doi: <http://doi.org/10.1002/adma.202301627>. PubMed PMID: 36960816.
- [3] WU, G., PANAHI-SARMAD, M., XIAO, X., *et al.*, "Fabrication of capacitive pressure sensor with extraordinary sensitivity and wide sensing range using PAM/BIS/GO nanocomposite hydrogel and conductive fabric", *Composites. Part A, Applied Science and Manufacturing*, v. 145, n. 106373, pp. 106373, 2021. doi: <http://doi.org/10.1016/j.compositesa.2021.106373>.
- [4] ZHANG, T., DING, Y., HU, C., *et al.*, "Self-powered stretchable sensor arrays exhibiting magnetoelasticity for real-time human-machine interaction", *Advanced Materials*, v. 35, n. 50, pp. e2203786, Jun. 2023. doi: <http://doi.org/10.1002/adma.202203786>. PubMed PMID: 35701188.
- [5] AHMAD, J., YASEEN, M., ALI, M., *et al.*, "Designing copper-nickel hybrid nanoparticles based resistive sensor for ammonia gas sensing.", *Materials Chemistry and Physics*, v. 305, pp. 127868, 2023. doi: <http://doi.org/10.1016/j.matchemphys.2023.127868>.
- [6] SINHA, M., NEOGI, S., GHOSH, R., "Temperature dependent selectivity switching from methanol to formaldehyde using ZnO nanorod based chemi-resistive sensor.", *Sensors and Actuators. A, Physical*, v. 357, pp. 114405, 2023. doi: <http://doi.org/10.1016/j.sna.2023.114405>.
- [7] NIE, L., ZHANG, L., DI, X., *et al.*, "Assembly of highly-sensitive capacitive flexible pressure sensor based on BTO NWs-TPU porous composites film.", *Vacuum*, v. 205, pp. 111423, 2022. doi: <http://doi.org/10.1016/j.vacuum.2022.111423>.
- [8] ZHAO, Y., GUO, X., HONG, W., *et al.*, "Biologically imitated capacitive flexible sensor with ultrahigh sensitivity and ultralow detection limit based on frog leg structure composites via 3D printing", *Composites Science and Technology*, v. 231, pp. 109837, 2023. doi: <http://doi.org/10.1016/j.compscitech.2022.109837>.
- [9] YU, Y., CUI, X., LIANG, Z., *et al.*, "Monitoring of three-dimensional resin flow front using hybrid piezoelectric-fiber sensor network in a liquid composite molding process", *Composites Science and Technology*, v. 229, pp. 109712, 2022. doi: <http://doi.org/10.1016/j.compscitech.2022.109712>.
- [10] ZHOU, P., ZHENG, Z., WANG, B., *et al.*, "Self-powered flexible piezoelectric sensors based on self-assembled 10 nm BaTiO₃ nanocubes on glass fiber fabric", *Nano Energy*, v. 99, pp. 107400, 2022. doi: <http://doi.org/10.1016/j.nanoen.2022.107400>.
- [11] LEE, M.H., KIM, D.J., CHOI, H.I., *et al.*, "Thermal quenching effects on the ferroelectric and piezoelectric properties of BiFeO₃-BaTiO₃ ceramics", *ACS Applied Electronic Materials*, v. 1, n. 9, pp. 1772–1780, 2019. doi: <http://doi.org/10.1021/acsaelm.9b00315>.

- [12] YU, C., LIU, K., XU, J., *et al.*, “High-performance multifunctional piezoresistive/piezoelectric pressure sensor with thermochromic function for wearable monitoring”, *Chemical Engineering Journal*, v. 459, pp. 141648, 2023. doi: <http://doi.org/10.1016/j.cej.2023.141648>.
- [13] PARK, H., OH, S.J., KIM, M., *et al.*, “Plasticizer structural effect for sustainable and high-performance PVC gel-based triboelectric nanogenerators”, *Nano Energy*, v. 114, pp. 108615, 2023. doi: <http://doi.org/10.1016/j.nanoen.2023.108615>.
- [14] VÁZQUEZ-LÓPEZ, A., AO, X., DEL RÍO SAEZ, J.S., *et al.*, “Triboelectric nanogenerator (TENG) enhanced air filtering and face masks: Recent advances”, *Nano Energy*, v. 114, pp. 108635, 2023. doi: <http://doi.org/10.1016/j.nanoen.2023.108635>.
- [15] KOBAYASHI, M., OGINO, H., BURMAN, M., *et al.*, “Shape sensing for CFRP and aluminum honeycomb sandwich panel using inverse finite element method with distributed fiber-optic sensors”, *Composite Structures*, v. 308, pp. 116648, 2023. doi: <http://doi.org/10.1016/j.compstruct.2022.116648>.
- [16] LIU, Y., CHEN, Y., LI, C., *et al.*, “Copper-multiwalled carbon nanotubes decorated fiber-optic surface plasmon resonance sensor for detection of trace hydrogen sulfide gas”, *Optical Fiber Technology*, v. 76, pp. 103221, 2023. doi: <http://doi.org/10.1016/j.yofte.2022.103221>.
- [17] SUN, X., LIU, T., ZHOU, J., *et al.*, “Recent applications of different microstructure designs in high performance tactile sensors: a review”, *IEEE Sensors Journal*, v. 21, n. 9, pp. 10291–10303, 2021. doi: <http://doi.org/10.1109/JSEN.2021.3061677>.
- [18] LI, R., ZHOU, Q., BI, Y., *et al.*, “Research progress of flexible capacitive pressure sensor for sensitivity enhancement approaches.”, *Sensors and Actuators. A, Physical*, v. 321, pp. 112425, 2021. doi: <http://doi.org/10.1016/j.sna.2020.112425>.
- [19] LI, M., GUAN, Q., LI, C., *et al.*, “Self-powered hydrogel sensors”, *Device*, v. 1, n. 1, pp. 100007, 2023. doi: <http://doi.org/10.1016/j.device.2023.100007>.
- [20] ZHANG, Z., LIU, G., LI, Z., *et al.*, “Flexible tactile sensors with biomimetic microstructures: mechanisms, fabrication, and applications”, *Advances in Colloid and Interface Science*, v. 320, pp. 102988, 2023. doi: <http://doi.org/10.1016/j.cis.2023.102988>. PubMed PMID: 37690330.
- [21] ZHANG, C., LIU, S., HUANG, X., *et al.*, “A stretchable dual-mode sensor array for multifunctional robotic electronic skin”, *Nano Energy*, v. 62, pp. 164–170, 2019. doi: <http://doi.org/10.1016/j.nanoen.2019.05.046>.
- [22] ADHIKARI, P.R., ISLAM, M.N., JIANG, Y., *et al.*, “Reverse electrowetting-on-dielectric energy harvesting using 3-D printed flexible electrodes for self-powered wearable sensors”, *IEEE Sensors Letters*, v. 6, n. 5, pp. 1–4, 2022. doi: <http://doi.org/10.1109/LSENS.2022.3170207>.
- [23] WEI, B., CHEN, G., WANG, Q., “A high-performance flexible piezoresistive sensor based on a nanocellulose/carbon-nanotube/polyvinyl-alcohol composite with a wrinkled microstructure”, *IEEE Sensors Journal*, v. 22, n. 16, pp. 15834–15843, 2022. doi: <http://doi.org/10.1109/JSEN.2022.3189053>.
- [24] ZHANG, W., SUN, W., XIAO, W., *et al.*, “Numerical simulation analysis of microstructure of dielectric layers in capacitive pressure sensors”, *IEEE Sensors Journal*, v. 19, n. 9, pp. 3260–3266, 2019. doi: <http://doi.org/10.1109/JSEN.2019.2893336>.
- [25] OSMAN, A., LU, J., “3D printing of polymer composites to fabricate wearable sensors: a comprehensive review”, *Materials Science and Engineering R Reports*, v. 154, pp. 100734, 2023. doi: <http://doi.org/10.1016/j.mser.2023.100734>.
- [26] GOULART, F.F., RIBEIRO, A.A., WAY, D.V., *et al.*, “Study of the influence of titanium and niobium particle size on the Ti35Nb alloy production with controlled porosity”, *Matéria (Rio de Janeiro)*, v. 27, n. 4, pp. e20220072, 2022. doi: <http://doi.org/10.1590/1517-7076-rmat-2022-0072>.
- [27] YU, S., LI, J., ZHAO, L., *et al.*, “Stretch-insensitive capacitive pressure sensor based on highly stretchable CuNWs electrode”, *Sensors and Actuators. A, Physical*, v. 346, pp. 113868, 2022. doi: <http://doi.org/10.1016/j.sna.2022.113868>.
- [28] GAO, F., ZHANG, K., GUO, Y., *et al.*, “(Ba, Sr) TiO₃/polymer dielectric composites-progress and perspective”, *Progress in Materials Science*, v. 121, pp. 100813, 2021. doi: <http://doi.org/10.1016/j.pmatsci.2021.100813>.
- [29] TANG, X., GU, Q., GAO, P., *et al.*, “Ultra-sensitive wide-range small capacitive pressure sensor based on porous CCTO-PDMS membrane”, *Sensors and Actuators Reports*, v. 3, pp. 100027, 2021. doi: <http://doi.org/10.1016/j.snr.2021.100027>.

- [30] ZHAO, J., CHEN, M., TAN, Q., “Embedding nanostructure and colossal permittivity of TiO₂-covered CCTO perovskite materials by a hydrothermal route”, *Journal of Alloys and Compounds*, v. 885, pp. 160948, 2021. doi: <http://doi.org/10.1016/j.jallcom.2021.160948>.
- [31] RIBEIRO, A.V.S., DA SILVA, J.M., GLEIZE, P.J.P., “Análise da dispersão de nanotubos de carbono de paredes múltiplas com diferentes aditivos dispersantes”, *Matéria (Rio de Janeiro)*, v. 27, n. 3, pp. e20220063, 2022. doi: <http://doi.org/10.1590/1517-7076-rmat-2022-0063>.
- [32] ZHENG, Z., TAO, J., FANG, X., *et al.*, “Life and failure of oriented carbon nanotubes composite electrode for resistance spot welding”, *Matéria (Rio de Janeiro)*, v. 28, n. 1, pp. e20230005, 2023. doi: <http://doi.org/10.1590/1517-7076-rmat-2023-0005>.
- [33] LIU, F., DAI, S., CAO, J., *et al.*, “CNTs based capacitive stretchable pressure sensor with stable performance”, *Sensors and Actuators. A, Physical*, v. 343, pp. 113672, 2022. doi: <http://doi.org/10.1016/j.sna.2022.113672>.
- [34] WU, X., ZHAO, W., DUAN, J., *et al.*, “Flexible pressure sensor based on graphene/PS microsphere/PDMS composite dielectric layer and activated carbon non-woven fabrics”, *Materials Letters*, v. 326, pp. 132952, 2022. doi: <http://doi.org/10.1016/j.matlet.2022.132952>.
- [35] HWANG, J., KIM, Y., YANG, H., *et al.*, “Fabrication of hierarchically porous structured PDMS composites and their application as a flexible capacitive pressure sensor”, *Composites. Part B, Engineering*, v. 211, pp. 108607, 2021. doi: <http://doi.org/10.1016/j.compositesb.2021.108607>.
- [36] MA, Z., ZHANG, K., YANG, S., *et al.*, “High-performance capacitive pressure sensors Fabricated by introducing dielectric filler and conductive filler into a porous dielectric layer through a Biomimic strategy”, *Composites Science and Technology*, v. 227, pp. 109595, 2022. doi: <http://doi.org/10.1016/j.compscitech.2022.109595>.